Journal of Geophysical Research: Space Physics

RESEARCH ARTICLE
10.1029/2018JA025393

Statistical Results of Multiband Chorus by Using THEMIS Waveform Data

Xinliang Gao[1,2], **Quanming Lu**[1,2], **and Shui Wang**[1,2]

[1]CAS Key Laboratory of Geospace Environment, Department of Geophysics and Planetary Science, University of Science and Technology of China, Hefei, China, [2]Collaborative Innovation Center of Astronautical Science and Technology, Harbin, China

Key Points:
- Based on their spectrograms, multiband chorus in the magnetosphere have been classified into two categories: EM-MBC and QE-MBC events
- Their distribution, amplitude, wave normal angles, and contribution to upper-band chorus in the Earth's magnetosphere, are presented
- Our study provides the first statistical results of MBC and also reveals a key role of lower band cascade in exciting upper-band chorus

Correspondence to:
Q. Lu,
qmlu@ustc.edu.cn

Citation:
Gao, X., Lu, Q., & Wang, S. (2018). Statistical results of multiband chorus by using THEMIS waveform data. *Journal of Geophysical Research: Space Physics*, *123*, 5506–5515. https://doi.org/10.1029/2018JA025393

Received 23 FEB 2018
Accepted 24 JUN 2018
Accepted article online 3 JUL 2018
Published online 24 JUL 2018

Abstract In this paper, we have studied thousands of multiband chorus events in the Earth's magnetosphere by utilizing seven-year THEMIS waveform data. There are two types of multiband chorus events in the magnetosphere: electromagnetic multiband chorus (EM-MBC) event, where two-band structure is found in both magnetic and electric spectrograms, and quasi-electrostatic multiband chorus (QE-MBC) event, where two-band structure is only detected in the electric spectrogram. EM-MBC events preferentially occur at low L-shells on the nightside but at high L-shells on the dayside. In EM-MBC events, lower-band waves typically have relatively larger magnetic amplitudes (>100 pT) and finite wave normal angles (10°–30°). The magnetic amplitudes of upper-band harmonic waves are found to be typically smaller than 30 pT and peak in the range of <5 pT. QE-MBC events tend to be detected at low L-shells on both dayside and nightside. They distribute mainly at relatively higher magnetic latitudes (6° to 15°) in the dawn sector. Lower-band chorus in QE-MBC events are typically highly oblique with very large wave normal angles (>60°), and their electric amplitudes peak in the range of 5–15 mV/m. For upper-band harmonic waves, their electric amplitudes mainly concentrate in the range of 0.15–0.5 mV/m. MBC events occupy a large population in upper-band chorus observed in the magnetosphere, which even contribute nearly half of upper-band chorus within $L < 10R_E$. Our study not only provides the first statistical results of MBC events but also reveals the significant role of the lower band cascade in generating upper-band chorus waves in the magnetosphere.

1. Introduction

Since the first report of chorus waves in 1960s (Burtis & Helliwell, 1969), they have long been a hot topic in magnetospheric physics. Whistler mode chorus wave is the most significant natural emission in the Earth's magnetosphere to regulate electron dynamics in the Van Allen radiation belt. They can not only refill the radiation belt by accelerating energetic electrons to relativistic energies (Reeves et al., 2013; Thorne et al., 2013; Xiao et al., 2014) but also cause the diffuse aurora through scattering low-energy electrons into the atmosphere (Ni et al., 2011; Thorne et al., 2010). Based on the linear theory and satellite observations, the major source region of chorus waves is considered to be very near the magnetic equator (Cully et al., 2011; Kennel & Petschek, 1966; Santolík et al., 2005). In the magnetosphere, chorus waves usually appear as either discrete rising/falling tones or hiss-like emissions in the dynamic spectrogram (Gao et al., 2014; Li et al., 2012). Chorus waves are typically observed to be quasi-parallel with very small wave normal angles (WNAs), but there is also a significant population of oblique waves with large WNs (Li et al., 2013). Moreover, they are typically divided into two bands by a power gap around $0.5f_{ce}$ (where f_{ce} is the equatorial electron gyrofrequency; Burtis & Helliwell, 1969): lower band (0.1–0.5 f_{ce}) and upper band (0.5–0.8 f_{ce}).

The remarkable two-band spectral structure of chorus waves has remained a big challenge since past several decades. Although lower-band chorus waves have been commonly believed to be excited by anisotropic hot electrons in both linear and nonlinear ways (Gao et al., 2014; Gary et al., 2000; Ke et al., 2017; Lu et al., 2004, 2010; Omura et al., 2008), the generation mechanism of upper-band chorus waves is still under debate. The more direct idea is that upper-band whistler mode waves can be either linearly or nonlinearly generated by anisotropic warm (approximately hundreds of eV) electrons just like lower-band waves (Fu et al., 2014; Omura et al., 2009), but this will require an unrealistic temperature anisotropy of thermal electrons in the magnetosphere (Fu et al., 2014). Recently, Gao et al. (2016) reported two special chorus events, named as multiband chorus, where upper-band waves are just harmonics of lower-band waves. Then, they proposed a new mechanism to explain this multiband chorus wave, named as lower band cascade, and further suggested that this could be a potential generation mechanism of upper-band chorus waves. In this scenario, the

upper-band harmonic waves are generated through the nonlinear coupling between the electromagnetic and electrostatic components of lower-band chorus waves. With a 1-D PIC simulation model, Gao et al. (2017) and Chen et al. (2017) have successfully reproduced multiband chorus waves, and further confirmed this lower band cascade mechanism. Through theoretical analysis, Gao et al. (2018) have also obtained the explicit nonlinear driven force of the lower band cascade and predicted the existence of two types of multiband chorus waves in the magnetosphere: Type I events have two-band structure in both magnetic and electric spectrograms, and Type II events only show two-band structure in the electric spectrogram.

In this paper, we present the first statistical results of multiband chorus waves in the Earth's magnetosphere by analyzing about seve-year (June 2008 to June 2015) THEMIS waveform data. Based on their spectrograms, multiband chorus waves have been classified into two categories: electromagnetic multiband chorus (EM-MBC) and quasi-electrostatic multiband chorus (QE-MBC). We have studied the global distribution, amplitude, and WNAs for two types of multiband chorus events and also roughly quantified their contribution to upper-band chorus waves in the Earth's magnetosphere. In section 2, we will introduce THEMIS instruments and data set used in this study. The method utilized for classifying multiband chorus events is described in section 3.1, and their statistical results are presented in section 3.2. In section 4, we summarize and further discuss our principal results.

2. THEMIS Instruments and Data Sets

The multiband chorus waves analyzed in this paper are captured by three inner THEMIS probes (A, D, and E) (Angelopoulos, 2008), whose orbit ideally covers the major source region of chorus waves. The THEMIS probes can simultaneously measure both electric and magnetic fields with a high sampling frequency ~16 kHz by Electric Field Instrument (Bonnell et al., 2008) and Search-Coil Magnetometer (Roux et al., 2008). However, only several waveform bursts will be recorded per day. Each waveform data lasts about 6–8 s, and its sampling frequency is adjusted to ~8 kHz. For each waveform data, we will conduct a 256-point FFT with a 128-point moving window to analyze both magnetic and electric fields. Therefore, the obtained dynamic spectrogram will have a time resolution of ~0.016 s. While, the background magnetic field is measured by the Fluxgate Magnetometer with a sampling frequency of ~4 Hz (Auster et al., 2008). First, the waveform data are needed to be rotated into the field-aligned coordinate system, where z axis is along the background magnetic field, x axis is perpendicular to both azimuthal vector in the solar magnetic coordinate and z axis, and y axis completes the triad. Then, following the procedure developed by Bortnik et al. (2007), we can obtain the WNAs by analyzing three-dimensional magnetic fields. Since only magnetic fields are used during this calculation, the obtained WNAs have an inherent 180° ambiguity (Bortnik et al., 2007). So we have converted all WNAs into values less than 90°. The Poynting vector is calculated by using full magnetic and electric fields, which is then utilized to determine the propagating direction of chorus waves by the same method as described in previous works (Li et al., 2013).

3. Observational Results

3.1. Event Selection

The data set analyzed in this paper is collected from waveform data (scm and efw files) of three inner THEMIS probes (A, D, and E), covering the main source region of chorus waves between 4 and 12 R_E at all MLT. Since the orbit of THEMIS spacecraft is designed in the near-equatorial region, all selected events are confined to low magnetic latitudes, typically less than ±20°. The time range is from June 2008 to June 2015.We have identified two type of multiband chorus according to their spectrograms. Multiband chorus events show two-band structure in both magnetic and electric spectrograms; we name them as EM-MBC events. While, multiband chorus events are named as QE-MBC events for only exhibiting two-band structure in their electric spectrograms. Their detailed characteristics are exhibited in Figures 1 and 2.

Figure 1 shows a representative example of EM-MBC events, including (a) electric and (b) magnetic dynamic spectrograms, (c) magnetic amplitudes, (d) electric amplitudes, (e) frequencies, (f) WNAs, and (g) flags indicating the direction of Poynting vector (Pflag) for lower band (black points), upper band (gray points) and the second harmonic of lower band (red points), respectively. In Figures 1a, 1b, and 1e, the white or black dashed line marks the frequency of $0.5f_{ce}$. At each time, we first find the peak frequencies with the maximum magnetic power for both lower ($0.1f_{ce} < f_l < 0.5f_{ce}$) and upper ($0.5f_{ce} < f_u < f_{ce}$) bands and also get the

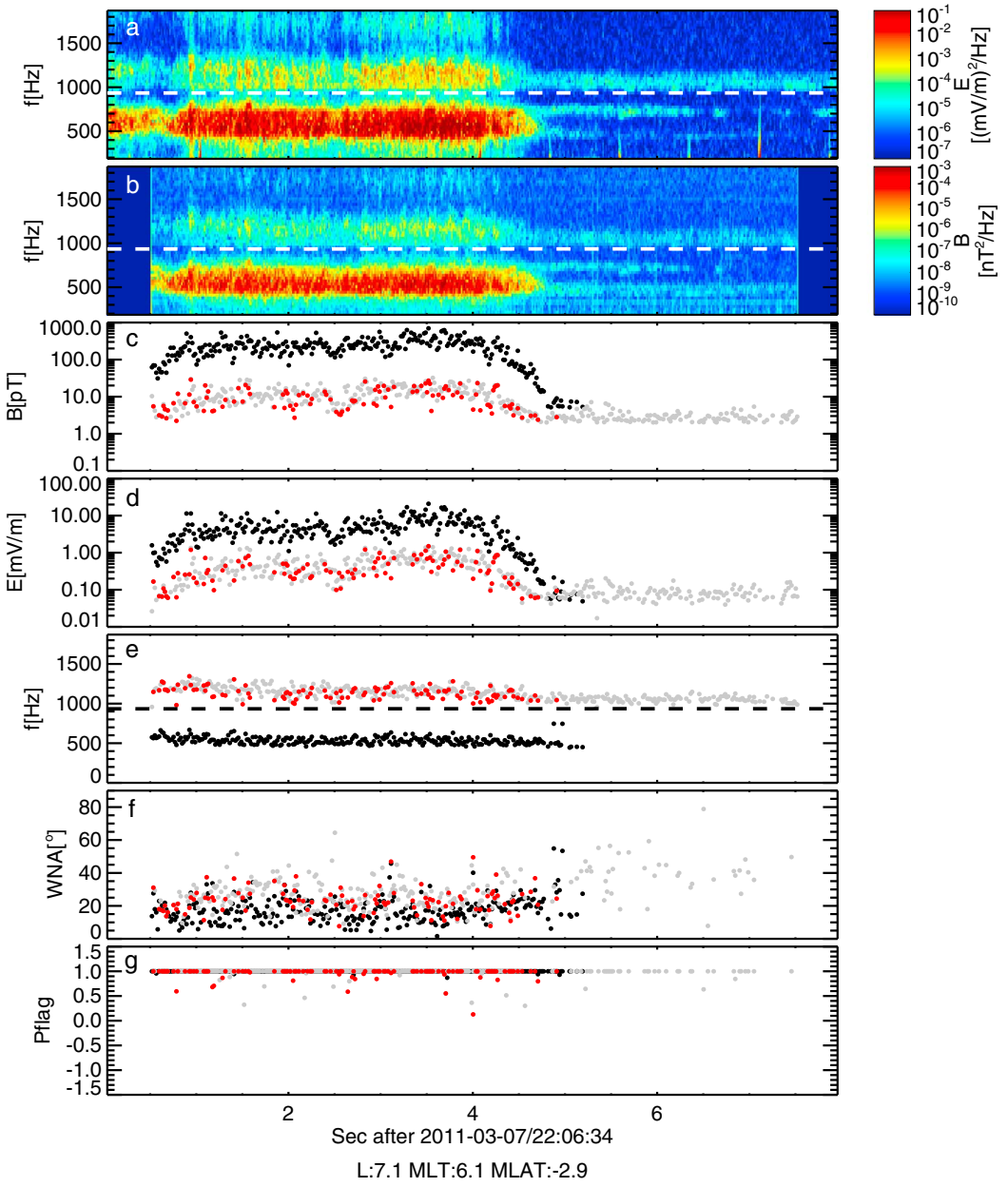

Figure 1. (a) Electric and (b) magnetic dynamic spectrograms, (c) magnetic amplitudes, (d) electric amplitudes, (e) frequencies, (f) wave normal angles (WNAs), and (g) flags indicating the direction of Poynting vector (Pflag) for lower band (black points), upper band (gray points), and the second harmonic of lower band (red points), respectively, in an example of EM-MBC events. In Figures 1a, 1b, and 1e, the white or black dashed line marks the frequency of $0.5f_{ce}$.

frequency of the second harmonic ($f_h = 2f_l$). Then, we calculate the magnetic (or electric) amplitude by integrating the magnetic (or electric) power over three adjacent bins around each characteristic frequency (f_l, f_u, or f_h). Meanwhile, we can also obtain the average frequency (f_{la}, f_{ua}, or f_{ha}), WNA (θ_{la}, θ_{ua}, or θ_{ha}), and flag (P_{la}, P_{ua}, or P_{ha}) weighted by the magnetic power over three adjacent bins around each characteristic frequency. At each time, the individual flag of each frequency bin is given as either 1 or −1 according to the propagating direction of the wave mode, where 1 means propagating away from the magnetic equator, and −1 denotes propagating toward the magnetic equator. However, upper and lower bands typically have a finite bandwidth, which means each band comprises of several frequency bins with different individual flags (−1 or 1). To define the propagating direction of each band, we then calculate the average flag (i.e., P_{la}, P_{ua}, or P_{ha}) weighted by the magnetic power over three adjacent bins around

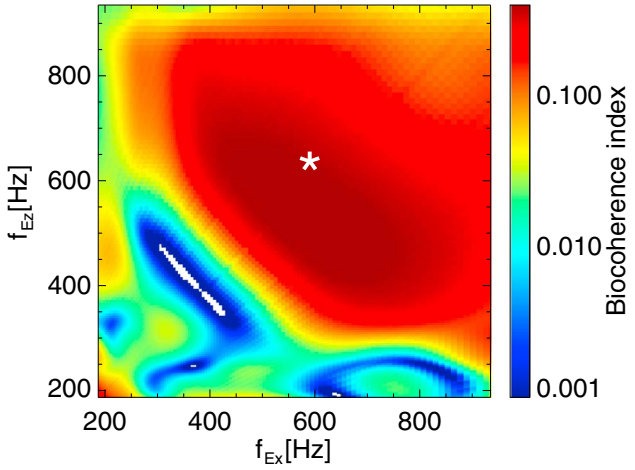

Figure 2. The distribution of the bicoherence index. The white star denotes the peak frequency of the lower band at the middle time of the selected time interval.

each characteristic frequency (f_l, f_u, or f_h). Figure 1g shows the weighted flag for each band, which now becomes a value between −1 and 1. Here the positive flag means propagating away from the equator, while the negative flag means propagating toward the equator. Further, at each time, we only record the data points satisfying the following criteria. For lower band, its magnetic amplitude should be larger than 5 pT, while, for upper band, its magnetic amplitude should be larger than 2 pT. According to previous works (Gao et al., 2016, 2017), the harmonic upper-band waves excited through the lower band cascade will have the same WNA and propagating direction as the lower-band waves. Therefore, for the second harmonic, we require its magnetic amplitude larger than 2 pT,$|\theta_{ha} - \theta_{la}|<10°$, $P_{ha}\times P_{la} > 0$, and $f_{ha} > 0.5f_{ce}$. Finally, if there are at least 30, 20, and 10 data points for lower band, upper band, and the second harmonic, respectively, in one 6- to 8-s waveform data, then we record it as a "potential" EM-MBC event, which will be further checked by the bicoherence analysis as shown in Figure 2. In this procedure, we actually first pick chorus events simultaneously having both lower and upper bands, and then identify upper-band harmonic waves in those chorus events. As shown in Figure 1, there is much overlap between the data points for the second harmonic (red) and upper band (gray). But the number of data points for the second harmonic is usually smaller than those for upper band, which is mainly due to the strict criteria applied to finding upper-band harmonic waves in this study.

The dynamic spectrograms in Figures 1a and 1b exhibit very clear banded structure, which is separated roughly by a power gap at $0.5f_{ce}$. Unlike events reported by Gao et al. (2016), this EM-MBC event belongs to hiss-like emissions, indicating that the lower band cascade is a common process of whistler mode waves regardless of their time-frequency structures. In this event, the magnetic amplitude of the lower band is mainly larger than 100 pT, and the amplitude ratio between the lower band and its second harmonic is slightly larger than 1 order (Figure 1c). The lower-band chorus waves are propagating quasi-parallel to the background magnetic field, whose WNAs are around ~20° (Figure 1f). Just as expected, both lower band and its second harmonic are propagating in the same direction, that is, away from the magnetic equator (Figure 1g).

The bicoherence analysis is a useful method to check the phase coupling among three wave modes (Agapitov et al., 2015; Gao et al., 2016, 2017; van Milligen et al., 1995). The bicoherence index of this EM-MBC event is calculated for a time interval of 40 ms, whose middle time is determined by the data point with the median magnetic amplitude of the second harmonic. Figure 2 shows the distribution of the bicoherence index, which is defined as $\left|E_z(f_1)E_x(f_2)E_x^*(f_3)\right|^2/\left|E_z(f_1)E_x(f_2)\right|^2\left|E_x^*(f_3)\right|^2$ (where $f_3 = f_1 + f_2$ and the bracket $\langle\rangle$ denotes an average over the 40-ms interval). The peak frequency of the lower band at the middle time has been marked by a white star. The large bicoherence index shown in Figure 2 means there is a strong coupling among three wave modes, that is, $f_3 = f_1 + f_2$. We can clearly find that the large bicoherence index occurs in the region with 1,000 Hz $< f_3$ (i.e., $f_1 + f_2$) $<$ 1,500 Hz, which is consistent with the upper band shown in Figure 1a. For each potential EM-MBC event, if the bicoherence index marked by the white star is larger than 0.1, then we record it as an EM-MBC event.

Figure 3 presents an example of QE-MBC events in the same format as that in Figure 1. The banded structure can only be observed in the electric spectrogram (Figure 3a), while the magnetic spectrogram only exhibits lower-band falling tones (Figure 3b). Moreover, the lower-band chorus waves have very large WNAs as shown in Figure 3f. This provides a direct observational evidence for the theoretical prediction of QE-MBC events in the Earth's magnetosphere (Gao et al., 2018). Since the second harmonic is quasi-electrostatic, the criteria for classifying QE-MBC events are set as follows: for lower band, the magnetic amplitude $>$ 5 pT, and at least 30 data points; for the second harmonic, the magnetic amplitude $<$ 2 pT, the electric amplitude $>$ 0.1 mV/m, $f_{ha} > 0.5f_{ce}$, and at least 10 data points. Then, we have further checked the bicoherence index for the selected QE-MBC events as above. Finally, we have selected 1454 EM-MBC events and 732 QE-MBC events from 28,353 waveform data. Note that all multiband chorus events have also been visually checked to remove the anonymous noise.

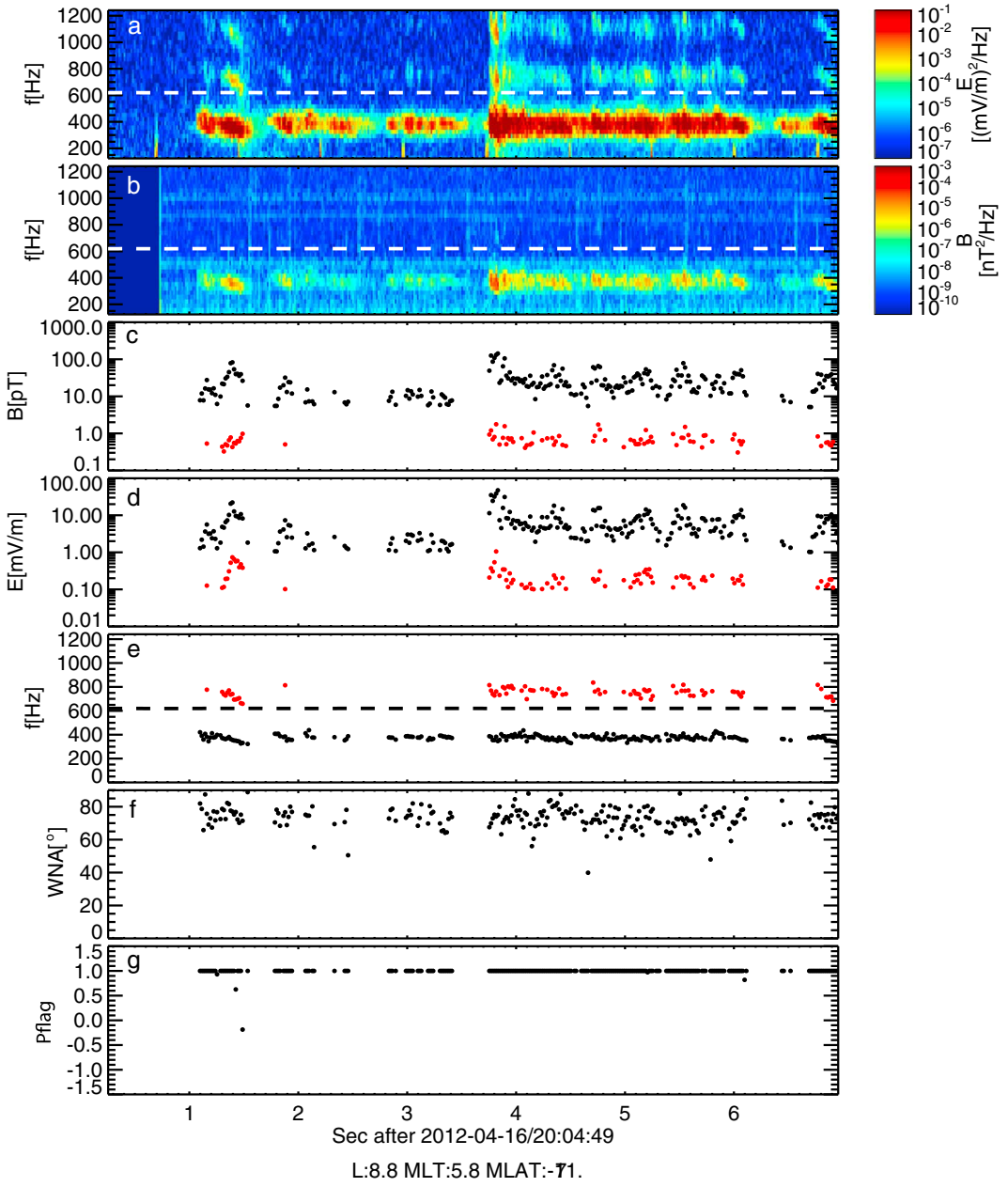

Figure 3. An example of QE-MBC events presented in the same format as that in Figure 1.

3.2. Statistical Results of Multiband Chorus

The global distribution in (a) L-MLT and (b)|MLAT|-MLT domains for total waveform data regardless of the presence of chorus waves is given in Figure 4. The color bars denote the number of samples. The waveform data collected from the past seven years provide fairly good coverage in L-MLT domain, but they are preferentially recorded at larger L-shells and on the dayside (Figure 4a). Since the orbit of THEMIS spacecraft is designed near the equatorial region, the majority of waveform data are confined to low MLAT, typically less than 20° (Figure 4b). To reduce the influence aroused by the inhomogeneous distribution of waveform data, we will show the occurrence rate instead of event number for both EM-MBC and QE-MBC events. In each bin, the occurrence rate is given by the ratio between the event number for each category and the number of waveform data in the same bin.

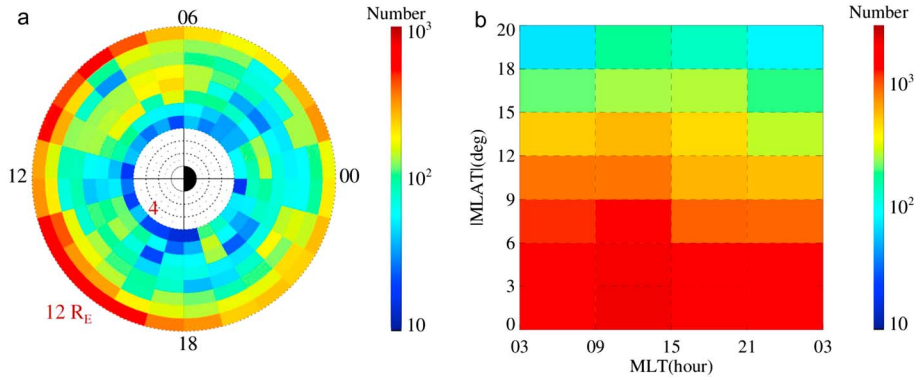

Figure 4. The global distribution in (a) L-MLT and (b) |MLAT|-MLT domains for total waveform data regardless of the presence of chorus waves. The bin size is 1 L × 1 h MLT.

Figure 5 gives the occurrence rate of EM-MBC events in (a) L-MLT and (b) |MLAT|-MLT domains. Overall, the multiband chorus event is a very common phenomenon related to whistler waves, which can be widely observed in the Earth's magnetosphere. In Figure 5a, we further find the EM-MBC event preferentially occurs at low L-shells on the nightside, while the high occurrence rate on the dayside tends to be at high L-shells. As expected, the EM-MBC events have a high occurrence rate at low magnetic latitude ($|MLAT| < 6°$) as shown in Figure 5b, which is commonly believed to be the major source region of lower-band chorus waves (Gao et al., 2014; Li et al., 2012). More interesting is that there is also a significant population of EM-MBC events detected at high magnetic latitude ($|MLAT| > 15°$). With the same format, the global distribution of occurrence rate for QE-MBC events is illustrated in Figure 6. The distribution of QE-MBC events is quite different from that of EM-MBC events. On the one hand, QE-MBC events are preferentially detected at low L-shells on both dayside and nightside (Figure 6a). On the other hand, the high occurrence rate of QE-MBC events is distributed mainly at relatively higher magnetic latitude (6° to 15°) in the dawn sector.

The statistical properties of selected multiband chorus events are also studied. For each multiband chorus event, the magnetic (or electric) amplitude of the second harmonic is given by the root mean square of all recorded amplitudes for the second harmonic. While, the WNA of the second harmonic is defined as the amplitude-weighted average WNA of all recorded points for the second harmonic. However, for the lower band, the calculation of its amplitude and WNA only involves those data points accompanied by the second harmonic. Therefore, we can further find out the condition for the upper-band harmonic chorus waves to be excited from lower-band waves through the lower band cascade in the Earth's magnetosphere. Figure 7 presents the occurrence rates of (a) magnetic amplitudes of the second harmonic, (b) WNAs of the lower band, and (c) magnetic amplitudes of the lower band for EM-MBC events. Here the occurrence rate is given by the ratio between the event number in one category and the total number of EM-MBC events. In Figure 7a, the magnetic amplitudes of upper-band harmonic waves are found to be typically smaller than 30 pT and to peak

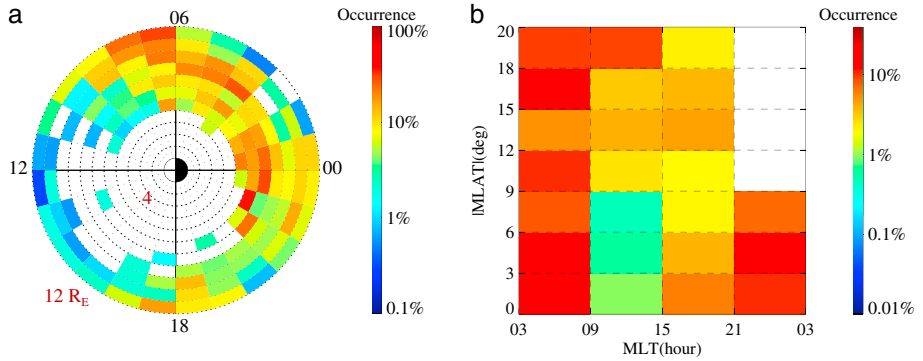

Figure 5. The occurrence rate of EM-MBC events in (a) L-MLT and (b) |MLAT|-MLT domains with a bin size of 1 L × 1 h MLT.

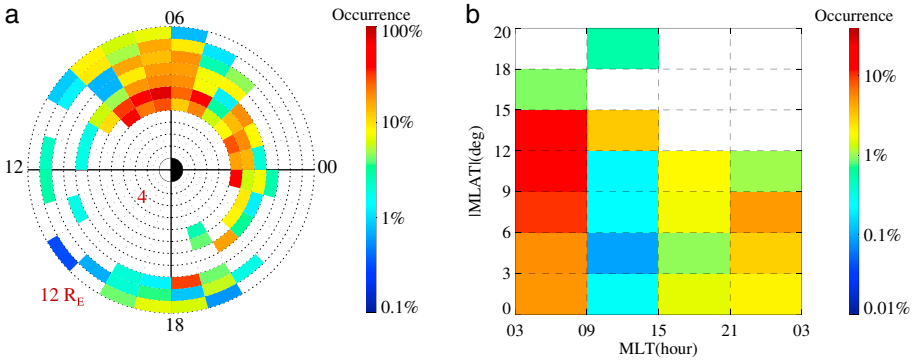

Figure 6. The occurrence rate of QE-MBC events in (a) L-MLT and (b) |MLAT|-MLT domains with a bin size of 1 L × 1 h MLT.

in the range of <5 pT. While, there are also some events having very large magnetic amplitudes (>50 pT). According to the previous statistical study by Li et al. (2011), lower-band chorus waves typically have very small WNAs in low-latitude regions, approximately peaking in the range of <10°. However, it is clearly shown that the lower-band waves with WNAs smaller than 10° are difficult to drive upper-band harmonic waves (Figure 7b) mainly due to their too weak electrostatic components in the parallel direction. Since the upper-band harmonic wave excited through the lower band cascade have the same WNA as the lower-band wave, then Figure 7b also tells that upper-band harmonic waves tend to have relatively larger WNAs (>10°), and their WNAs mainly concentrate in the range of 10°–30°. According to Figure 7c, it requires the magnetic amplitude of lower-band chorus waves roughly larger than 100 pT to excite upper-band harmonic waves through the lower band cascade.

The distributions of (a) electric amplitudes of the second harmonic, (b) WNAs of the lower band, and (c) electric amplitudes of the lower band for QE-MBC events are shown in Figure 8. For QE-MBC events, the magnetic amplitudes of upper-band harmonic waves are usually too weak to be detectable, but they have significant electric amplitudes mainly concentrating in the range of 0.15–0.5 mV/m (Figure 8a). Most remarkable, the lower-band chorus waves in QE-MBC events are typically highly oblique with very large WNAs (>60°) as displayed in Figure 8b. Similarly, the electric amplitudes of lower-band waves are also required to be sufficiently large, which peak in the range of 5–15 mV/m (Figure 8c).

The contribution of multiband chorus events to upper-band chorus waves in the Earth's magnetosphere is illustrated in Figure 9, showing the occurrence rates of UB events (upper-band chorus events excluded multiband chorus; red), EM-MBC events (blue), and QE-MBC events (yellow) in different L ranges. Here for each UB event, there are at least 20 data points for the upper band but less than 10 data points for the second harmonic. In other words, UB events shown in Figure 9 include chorus events only having upper band and two-band chorus events without containing upper-band harmonic waves. The number of UB events is 3173. The occurrence rate is defined as the ratio between the event number of each category and the event number of waveform data in the same L range. The value on the top of each bar denotes the percentage for each wave

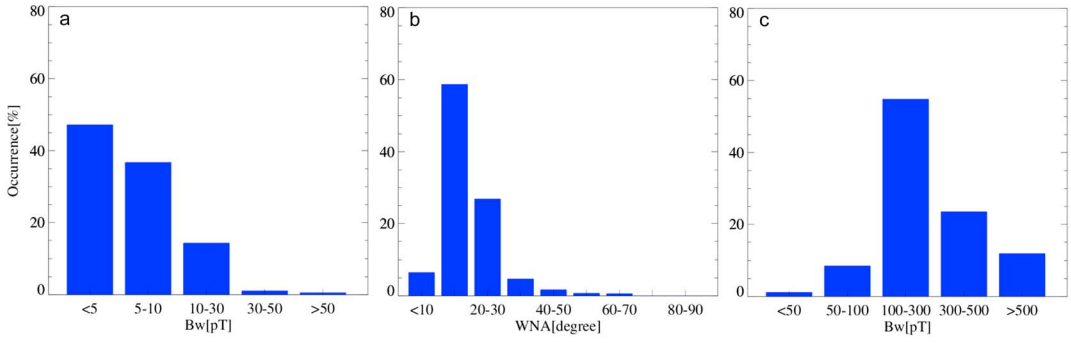

Figure 7. The occurrence rates of (a) magnetic amplitudes of the second harmonic, (b) wave normal angles of the lower band, and (c) magnetic amplitudes of the lower band for EM-MBC events.

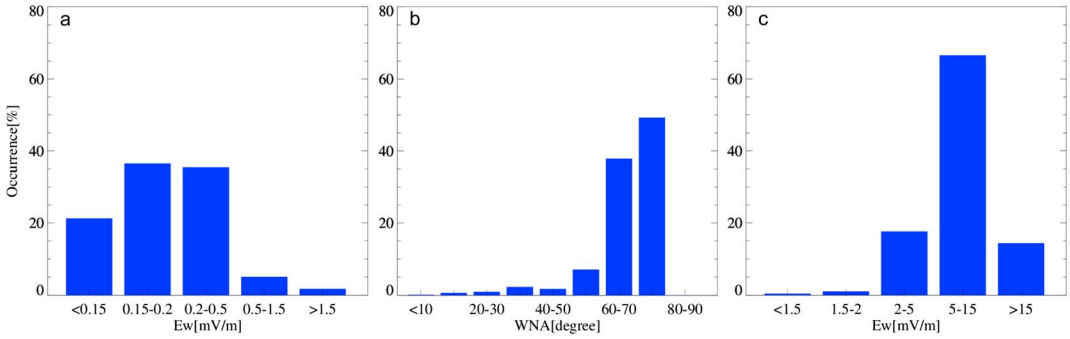

Figure 8. The occurrence rates of (a) magnetic amplitudes of the second harmonic, (b) wave normal angles of the lower band, and (c) magnetic amplitudes of the lower band for QE-MBC events.

category in one L range, which is given by the ratio between the event number of one category and the total event number in the same L range. In Figure 9, we can easily find that both UB and EM-MBC events have a similar trend, which are preferentially observed at relatively larger L-shells (>7 R_E). While, for QE-MBC events, their occurrence rate tends to decrease with the L-shell, which is consistent with their global distribution presented in Figure 6a. Most important of all, multiband chorus events (EM-MBC and QE-MBC events) occupy a very large population in upper-band chorus events observed in the magnetosphere. In particular, multiband chorus events can even contribute nearly half of upper-band chorus waves within L < 10 R_E.

4. Summary and Discussion

In this paper, we have analyzed thousands of multiband chorus events (both EM-MBC and QE-MBC events) in the Earth's magnetosphere collected from the seven-year waveform data of three inner THEMIS probes. This comprehensive study provides the first statistical results of multiband chorus events and reveals their significant contribution to upper-band chorus waves in the magnetosphere. The principal results are summarized as follows:

1. EM-MBC events preferentially occur at low L-shells on the nightside but at high L-shells on the dayside. They have a high occurrence rate at low magnetic latitude (|MLAT| < 6°). The magnetic amplitudes of upper-band harmonic waves are found to be typically smaller than 30 pT and peak in the range of <5 pT.
2. QE-MBC events tend to be detected at low L-shells on both dayside and nightside. And the high occurrence rate of QE-MBC events is distributed mainly at the relatively higher magnetic latitude (6° to 15°) in the dawn sector. The magnetic amplitudes of upper-band harmonic waves are usually too weak to be detectable, but they have significant electric amplitudes mainly concentrating in the range of 0.15–0.5 mV/m.
3. To excite EM-MBC events, lower-band chorus waves are required to have relatively large magnetic amplitudes (≳100 pT) and finite WNAs (10°–30°). While, lower-band chorus waves in QE-MBC events are typically highly oblique with very large WNAs (>60°), and their electric amplitudes are also required to be sufficiently large, which peak in the range of 5–15 mV/m.
4. The multiband chorus waves are a very common phenomenon related to whistler waves, which can be widely observed in the Earth's magnetosphere. They have occupied a very large population in upper-band chorus events observed in the magnetosphere. In particular, multiband chorus events can even contribute nearly half of upper-band chorus waves within L < 10 R_E.

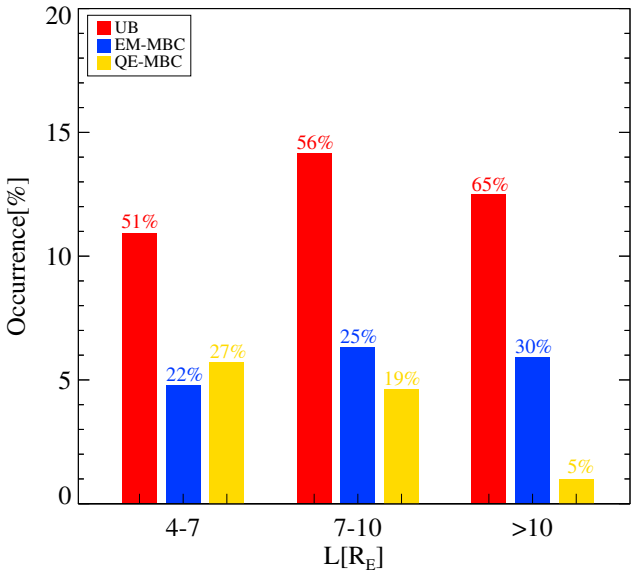

Figure 9. The occurrence rates of UB events (upper-band chorus events excluded multiband chorus) (red), EM-MBC events (blue), and QE-MBC events (yellow) in different L ranges. The value on the top of each bar denotes the percentage for each wave category in one L range.

Multiband chorus waves are first reported as special chorus events in the Earth's magnetosphere by Gao et al. (2016), where upper-band

waves are harmonics of lower-band chorus waves. Based on observational analysis and full particle simulations (Chen et al., 2017; Gao et al., 2016, 2017), multiband chorus waves have been well explained by the lower band cascade, which is also considered as a potential generation mechanism of upper-band chorus waves. Our statistical results have clearly shown that multiband chorus waves are a very common phenomenon related to whistler waves, which can be widely observed in the Earth's magnetosphere. Furthermore, the condition for the lower band cascade can be easily satisfied for a large population of lower-band chorus waves. Therefore, our study reveals that the lower band cascade is a very common and significant nonlinear process in controlling the evolution of whistler waves in the magnetosphere.

Multiband chorus waves have occupied a very large population in upper-band chorus events observed in the magnetosphere, which can even contribute nearly half of upper-band chorus waves within L $<$ 10 R_E. Moreover, they can account for two primary properties of upper-band chorus waves observed in the Earth's magnetosphere. Through the lower band cascade, upper-band harmonic waves are typically generated with magnetic amplitudes 1 to 2 orders smaller than lower-band waves, which can well explain why upper-band chorus waves are usually observed to be much weaker than lower band waves (Li et al., 2011). According to previous statistical results (Li et al., 2011), upper-band chorus waves tend to have relatively larger WNAs ($>$10°), while lower-band chorus waves have a very significant population with very small WNAs ($<$10°). This distinct difference between them can be explained by the lower band cascade in some degree. Based on previous works (Gao et al., 2016, 2018), the lower band cascade will become very weak if the WNA of the lower-band whistler wave is too small, since the electrostatic component of the lower-band wave is too weak. In other word, the lower band cascade tends to occur for lower-band chorus with a relatively larger WNA, which drives upper-band harmonic waves preferentially having a larger WNA. As a result, there will be a salient drop of occurrence rates for multiband chorus events (or upper-band chorus events) with WNA smaller than 10°. Therefore, our statistical results further suggest that the lower band cascade could be one significant potential mechanism to generate upper-band chorus ($>0.5f_{ce}$) in the Earth's magnetosphere.

It is worth noting that we have applied very strict criteria to picking multiband chorus events to ensure that the recorded data points for upper-band harmonic are correct. Therefore, not all data points for the second harmonic can be recorded, and their number is usually smaller than those for upper band in each multiband chorus event. Kellogg et al. (2010) also reported chorus waves with harmonic spectral structures, which can also be explained by the steepening mechanism (Yoon et al., 2014). Those chorus waves are typically quasi-electrostatic with very large wave amplitudes ($>$15 mV/m), which just belong to a small category ($>$15 mV/m in Figure 8c) of QE-MBC events.

Acknowledgments
This work was supported by the NSFC grants 41774151, 41631071, 41604128, and 41474125, Youth Innovation Promotion Association of the Chinese Academy of Sciences (2016395), and the Key Research Program of Frontier Sciences, CAS (QYZDJ-SSW-DQC010). We also acknowledge the entire THEMIS instrument group and the THEMIS data obtained from http://themis.ssl.berkeley.edu/data/themis.

References

Agapitov, O. V., Krasnoselskikh, V., Mozer, F. S., Artemyev, A. V., & Volokitin, A. S. (2015). Generation of nonlinear electric field bursts in the outer radiation belt through the parametric decay of whistler waves. *Geophysical Research Letters*, *42*, 3715–3722. https://doi.org/10.1002/2015GL064145

Angelopoulos, V. (2008). The THEMIS mission. *Space Science Reviews*, *141*(1-4), 5–34. https://doi.org/10.1007/s11214-008-9336-1

Auster, H. U., Glassmeier, K. H., Magnes, W., Aydogar, O., Baumjohann, W., Constantinescu, D., et al. (2008). The THEMIS fluxgate magnetometer. *Space Science Reviews*, *141*(1-4), 235–264. https://doi.org/10.1007/s11214-008-9365-9

Bonnell, J. W., Mozer, F. S., Delory, G. T., Hull, A. J., Ergun, R. E., Cully, C. M., et al. (2008). The Electric Field Instrument (EFI) for THEMIS. *Space Science Reviews*, *141*(1-4), 303–341. https://doi.org/10.1007/s11214-008-9469-2

Bortnik, J., Cutler, J. W., Dunson, C., & Bleier, T. E. (2007). An automatic wave detection algorithm applied to Pc1 pulsations. *Journal of Geophysical Research*, *112*, A04204. https://doi.org/10.1029/2006JA011900

Burtis, W. J., & Helliwell, R. A. (1969). Banded chorus a new type of VLF radiation observed in the magnetosphere by OGO 1 and OGO 3. *Journal of Geophysical Research*, *74*(11), 3002–3010. https://doi.org/10.1029/JA074i011p03002

Chen, H. Y., Gao, X. L., Lu, Q. M., Ke, Y. G., & Wang, S. (2017). Lower band cascade of whistler waves excited by anisotropic hot electrons: One-dimensional PIC simulations. *Journal of Geophysical Research: Space Physics*, *122*, 10,448–10,457. https://doi.org/10.1002/2017JA024513

Cully, C. M., Angelopoulos, V., Auster, U., Bonnell, J., & Le Contel, O. (2011). Observational evidence of the generation mechanism for rising-tone chorus. *Geophysical Research Letters*, *38*, L01106. https://doi.org/10.1029/2010GL045793

Fu, X., Cowee, M. M., Friedel, R. H., Funsten, H. O., Peter Gary, S., Hospodarsky, G. B., et al. (2014). Whistler anisotropy instabilities as the source of banded chorus: Van Allen Probes observations and particle-in-cell simulations. *Journal of Geophysical Research: Space Physics*, *119*, 8288. https://doi.org/10.1002/2014JA020364

Gao, X. L., Ke, Y. G., Lu, Q. M., Chen, L. J., & Wang, S. (2017). Generation of multiband chorus in the Earth's magnetosphere: 1-D PIC simulation. *Geophysical Research Letters*, *44*, 618–624. https://doi.org/10.1002/2016GL072251

Gao, X. L., Li, W., Thorne, R. M., Bortnik, J., Angelopoulos, V., Lu, Q. M., et al. (2014). New evidence for generation mechanisms of discrete and hiss-like whistler mode waves. *Geophysical Research Letters*, *41*, 4805–4811. https://doi.org/10.1002/2014GL060707

Gao, X. L., Lu, Q. M., Bortnik, J., Li, W., Chen, L. J., & Wang, S. (2016). Generation of multiband chorus by lower band cascade in the Earth's magnetosphere. *Geophysical Research Letters*, *43*, 2343–2350. https://doi.org/10.1002/2016GL068313

Gao, X. L., Lu, Q. M., Wang, S. J., & Wang, S. (2018). Theoretical analysis on lower band cascade as a mechanism for multiband chorus in the Earth's magnetosphere. *AIP Advances*, *8*(5), 055003. https://doi.org/10.1063/1.5025507

Gary, S. P., Winske, D., & Hesse, M. (2000). Electron temperature anisotropy instabilities: Computer simulations. *Journal of Geophysical Research*, *105*(A5), 10751–10759. https://doi.org/10.1029/1999JA000322

Ke, Y. G., Gao, X., Lu, Q., Wang, X., & Wang, S. (2017). Generation of rising-tone chorus in a two-dimensional mirror field by using the general curvilinear PIC code. *Journal of Geophysical Research: Space Physics*, *122*, 8154–8165. https://doi.org/10.1002/2017JA024178

Kellogg, P. G., Cattell, C. A., Goetz, K., Monson, S. J., & Wilson, L. B. III (2010). Electron trapping and charge transport by large amplitude whistlers. *Geophysical Research Letters*, *37*, L20106. https://doi.org/10.1029/2010GL044845

Kennel, C. F., & Petschek, H. E. (1966). Limit on stably trapped particle fluxes. *Journal of Geophysical Research*, *71*(1), 1–28. https://doi.org/10.1029/JZ071i001p00001

Li, W., Bortnik, J., Thorne, R. M., & Angelopoulos, V. (2011). Global distribution of wave amplitudes and wave normal angles of chorus waves using THEMIS wave observations. *Journal of Geophysical Research*, *116*, A12205. https://doi.org/10.1029/2011JA017035

Li, W., Bortnik, J., Thorne, R. M., Cully, C. M., Chen, L., Angelopoulos, V., et al. (2013). Characteristics of the Poynting flux and wave normal vectors of whistler-mode waves observed on THEMIS. *Journal of Geophysical Research: Space Physics*, *118*, 1461–1471. https://doi.org/10.1002/jgra.50176

Li, W., Thorne, R. M., Bortnik, J., Tao, X., & Angelopoulos, V. (2012). Characteristics of hiss-like and discrete whistler-mode emissions. *Geophysical Research Letters*, *39*, L18106. https://doi.org/10.1029/2012GL053206

Lu, Q. M., Wang, L. Q., Zhou, Y., & Wang, S. (2004). Electromagnetic instabilities excited by electron temperature anisotropy. *Chinese Physics Letters*, *21*, 129–132.

Lu, Q. M., Zhou, L. H., & Wang, S. (2010). Particle-in-cell simulations of whistler waves excited by an electron k distribution in space plasma. *Journal of Geophysical Research*, *115*, A02213. https://doi.org/10.1029/2009JA014580

Ni, B. B., Thorne, R. M., Shprits, Y. Y., Orlova, K. G., & Meredith, N. P. (2011). Chorus-driven resonant scattering of diffuse auroral electrons in nondipolar magnetic fields. *Journal of Geophysical Research*, *116*, A06225. https://doi.org/10.1029/2011ja016453

Omura, Y., Hikishima, M., Katoh, Y., Summers, D., & Yagitani, S. (2009). Nonlinear mechanisms of lower-band and upper-band VLF chorus emissions in the magnetosphere. *Journal of Geophysical Research*, *114*, A07217. https://doi.org/10.1029/2009JA014206

Omura, Y., Katoh, Y., & Summers, D. (2008). Theory and simulation of the generation of whistler mode chorus. *Journal of Geophysical Research*, *113*, A04223. https://doi.org/10.1029/2007ja012622

Reeves, G. D., Spence, H. E., Henderson, M. G., Morley, S. K., Friedel, R. H. W., Funsten, H. O., et al. (2013). Electron acceleration in the heart of the Van Allen radiation belts. *Science*, *341*(6149), 991–994. https://doi.org/10.1126/science.1237743

Roux, A., Le Contel, O., Coillot, C., Bouabdellah, A., de la Porte, B., Alison, D., et al. (2008). The search coil magnetometer for THEMIS. *Space Science Reviews*, *141*(1–4), 265–275. https://doi.org/10.1007/s11214-008-9455-8

Santolík, O., Gurnett, D. A., Pickett, J. S., Parrot, M., & Cornilleau-Wehirlin, N. (2005). Central position of the source region of storm-time chorus. *Planetary and Space Science*, *53*(1-3), 299–305. https://doi.org/10.1016/j.pss.2004.09.056

Thorne, R. M., Li, W., Ni, B., Ma, Q., Bortnik, J., Chen, L., et al. (2013). Rapid local acceleration of relativistic radiation-belt electrons by magnetospheric chorus. *Nature*, *504*(7480), 411–414. https://doi.org/10.1038/nature12889

Thorne, R. M., Ni, B., Tao, X., Horne, R. B., & Meredith, N. P. (2010). Scattering by chorus waves as the dominant cause of diffuse auroral precipitation. *Nature*, *467*(7318), 943–946. https://doi.org/10.1038/nature09467

van Milligen, B. P., Sanchez, E., Estrada, T., Hidalgo, C., Branas, B., Carreras, B., & Garcia, L. (1995). Wavelet bicoherence: A new turbulence analysis tool. *Physics of Plasmas*, *2*(8), 3017–3032. https://doi.org/10.1063/1.871199

Xiao, F., Yang, C., He, Z., Su, Z., Zhou, Q., He, Y., et al. (2014). Chorus acceleration of radiation belt relativistic electrons during March 2013 geomagnetic storm. *Journal of Geophysical Research: Space Physics*, *119*, 3325–3332. https://doi.org/10.1002/2014JA019822

Yoon, P. H., Pandey, V. S., & Lee, D.-H. (2014). Oblique nonlinear whistler wave. *Journal of Geophysical Research: Space Physics*, *119*, 1851–1862. https://doi.org/10.1002/2013JA018993